

Article

Molecular Modeling Based on Time-Dependent Density Functional Theory (TD-DFT) Applied to the UV-Vis Spectra of Natural Compounds

João Otávio Anhaia-Machado ^{1,†}, Artur Caminero Gomes Soares ^{1,†} , Claudinéia Aparecida Sales de Oliveira Pinto ¹ ,
Andres Ignacio Ávila Barrera ², André Rolim Baby ^{1,*}  and Gustavo Henrique Goulart Trossini ^{1,*} 

¹ Department of Pharmacy, Faculty of Pharmaceutical Sciences, University of Sao Paulo, Sao Paulo 05508-000, Brazil

² Department of Mathematics, Center for Modeling and Scientific Computing, Universidad de La Frontera, Temuco 4811230, Chile

* Correspondence: andrerb@usp.br (A.R.B.); trossini@usp.br (G.H.G.T.)

† These authors contributed equally to this work.

Abstract: As diseases caused by solar radiation have gained great prominence, several methods to prevent them have been developed. Among the most common, the use of sunscreens is customary and accessible. The application of theoretical methods has helped to design new compounds with therapeutic and protective functions. Natural compounds with described photoprotective potential properties (3-O-methylquercetin, gallic acid, aloin, catechin, quercetin, and resveratrol) were selected to perform theoretical studies. Computational methods were applied to predict their absorption spectra, using DFT and TD-DFT methods with functional B3LYP/6–311+g(d,p) basis sets and methanol (IEFPCM) as a solvent. The main electronic transitions of the compounds were evaluated by observing whether the differences in HOMO and LUMO energies that absorb in the UV range are UVA (320–400 nm), UVB (290–320 nm), or UVC (100–290 nm). Experimental validation was carried out for EMC, quercetin, and resveratrol, demonstrating the consistency of the computational method. Results obtained suggest that resveratrol is a candidate for use in sunscreens. The study provided relevant information about the in silico predictive power of natural molecules with the potential for use as photoprotective adjuvants, which may result in fewer time and resource expenditures in the search for photoprotective compounds.

Keywords: photoprotectors; natural products; molecular modeling; time-dependent density functional theory (TD-DFT); UV



Citation: Anhaia-Machado, J.O.; Soares, A.C.G.; de Oliveira Pinto, C.A.S.; Barrera, A.I.Á.; Baby, A.R.; Trossini, G.H.G. Molecular Modeling Based on Time-Dependent Density Functional Theory (TD-DFT) Applied to the UV-Vis Spectra of Natural Compounds. *Chemistry* **2023**, *5*, 41–53. <https://doi.org/10.3390/chemistry5010004>

Academic Editor: George Grant

Received: 23 November 2022

Revised: 19 December 2022

Accepted: 23 December 2022

Published: 28 December 2022



Copyright: © 2022 by the authors. Licensee MDPI, Basel, Switzerland. This article is an open access article distributed under the terms and conditions of the Creative Commons Attribution (CC BY) license (<https://creativecommons.org/licenses/by/4.0/>).

1. Introduction

A significant focus in public health has been placed on the risks caused by unprotected exposure to sun radiation, especially skin cancer, which has shown a significant increase in cases every year [1]. In light of this, studies to understand and develop better and safer photo-protective compounds for sunscreen formulations have become more desirable. Thus, it is necessary to expand the knowledge regarding compounds used in the prevention of the damage caused by ultraviolet (UV) radiation [2–4].

UV radiation is divided into three distinct categories according to their wavelength: UVA radiation (320–400 nm) is known to induce direct DNA damage, utilizing reactive oxygen species to create free radicals, which mostly lead to photoaging. UVB radiation (290–320 nm) has high energy, causes erythema and immunosuppression, and is associated with skin cancer. UVC radiation (100–290 nm) has especially high energy, making it extremely harmful to living beings; however, hardly any of it can get through the ozone layer present in the stratosphere. Therefore, UVB radiation is the one we are exposed to the most and the most harmful to human beings [5–8].

Among the main methods of preventing sun damage, the use of sunscreens is strongly recommended [9,10]. Sunscreens are composed of molecules that can absorb or reflect the sun's radiation in the UVA and UVB ranges. Currently, they are divided into two classes: organic, which can absorb solar radiation mostly in the UVA and UVB range, and inorganic, which act by scattering and reflecting UV radiation [11,12].

Consequently, because of its growing importance in everyday life, new strategies are being sought to develop better sunscreen formulations with wider UV coverage, more favorable aesthetics, greater adherence, and minimum skin penetration [13]. Computational studies utilizing molecular modeling methods have shown promising results in predicting the behavior of different compounds when interacting with UV radiation. This can be applied to extracting relevant information about the mechanism of action, understanding electronic transitions, and planning novel and potent compounds with photoprotective properties [14,15].

Molecular modeling is a group of computational methods that simulate physicochemical systems, seeking to generate, manipulate, and analyze realistic representations of molecular structures obtained from physicochemical properties calculated by computational chemistry techniques. Thereby, these methods can extract valuable information, which allows for a better understanding of the spectral, structural, and electronic behavior, that can be used to optimally plan for new compounds with the desired physicochemical properties [16,17].

Density functional theory (DFT) is a quantum mechanical method that assumes that all the system properties are charge density functions. This enables the calculation of the exact description of the structure, energy, and molecular properties of the compound. Utilizing DFT for excited states, the time-dependent density functional theory (TD-DFT) can obtain the electronic spectra for absorption and study several processes that involve the excited state [17–24].

Therefore, the main goals of this work were to study the electronic structures as well as the excited states of natural molecules to understand the electronic mechanism related to UV radiation absorption employing TD-DFT methods.

2. Materials and Methods

2.1. Dataset

Six compounds from natural sources with possible UV filter properties described in the literature were selected. Their chemical structures and names are presented in Table 1 [25–29].

The compound ethylhexyl methoxycinnamate (EMC) (Figure 1) was used as a reference for the study since it is a consolidated UVB filter [30–32].

Table 1. Compounds with two-dimensional (2D) structures and names.

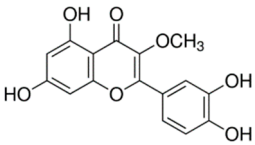
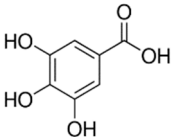
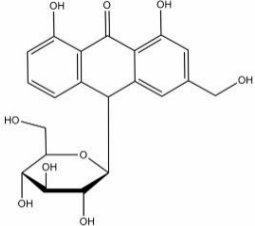
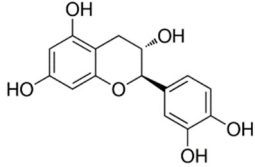
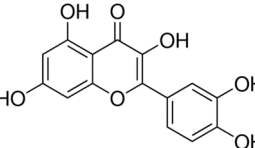
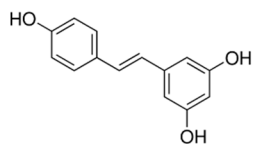
Compound	Structure
3-O-methylquercetin	
gallic acid	

Table 1. Cont.

aloin	
catechin	
quercetin	
resveratrol	

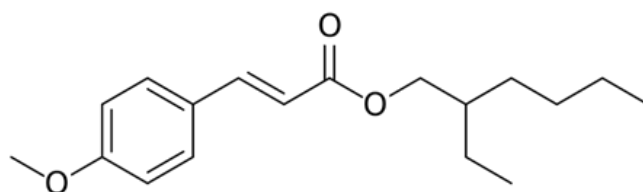


Figure 1. Ethylhexyl methoxycinnamate (EMC).

2.2. Computational Protocol

A UV spectra simulation was carried out for EMC and the natural compounds presented in Table 1. The protocol described in Figure 2 was applied individually for each compound.

The structural model construction was done with the program GaussView 4 [33]. After that, the compounds were submitted to conformational calculation in Spartan'14 [34], using the semi-empirical method PM6. The most stable conformation had its geometry optimized by the DFT method, with functional B3LYP and base 6-311+G(d,p) in Gaussian 09 [35–38]. The solvent effect used was evaluated by the methanol ($\epsilon = 32.61$) implicit solvent method IEFPCM, which was chosen because it is the same solvent employed in the experimental assay. The vibrational analysis was carried out in Gaussian 09 at the same theory level used in the geometrical optimizations, which ensures the local minimums are confirmed by the absence of an imaginary mode in the vibrational analysis calculations. Excited states were calculated with the TD-DFT method using the same functionals and base optimization calculations as the optimized geometry fundamental state. GaussView was used to extract the data regarding the epsilon coordinates (molar absorption) at the respective wavelengths from 100 to 500 nm, obtaining theoretical UV-vis absorption graphs. To validate the most suitable methodology to simulate the UV-vis, the calculation was performed for EMC, since it is the most commonly used UVB filter in sunscreen formulations and was used to validate the last studies published by the research group [14,39].

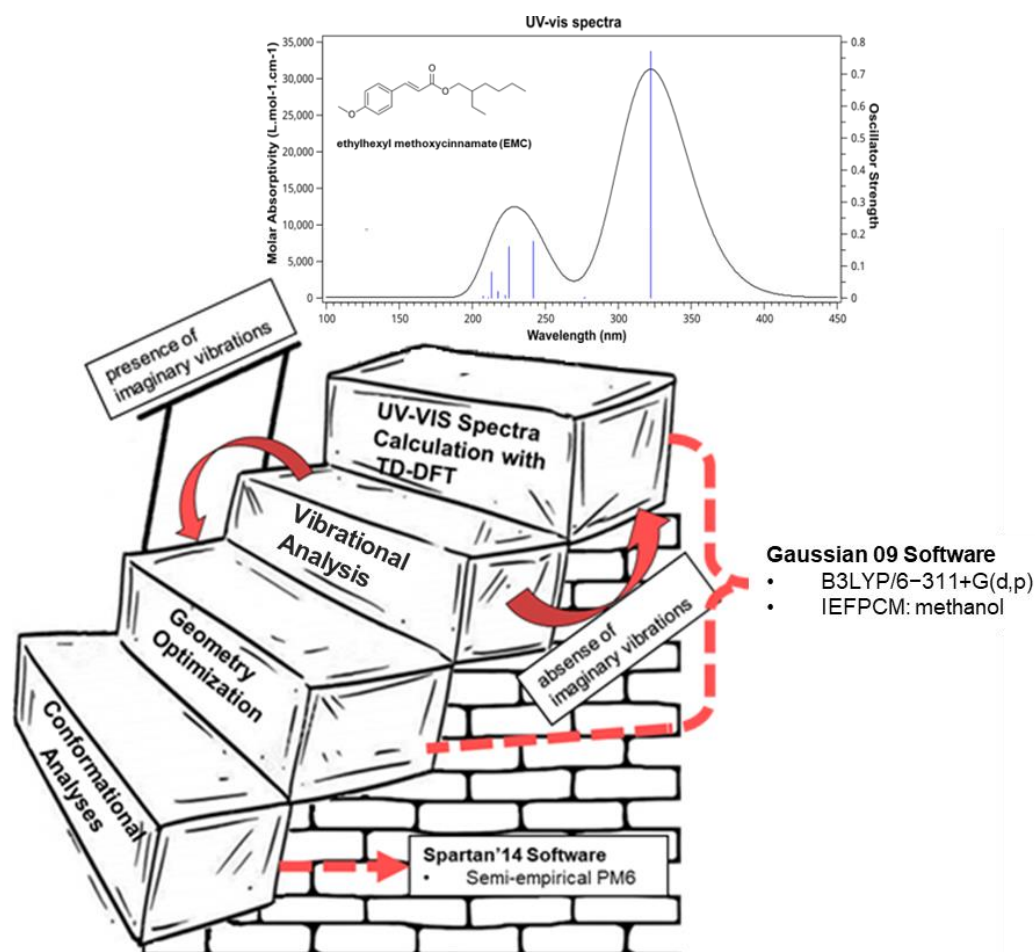


Figure 2. Computational protocol used to calculate the UV-vis spectra and electronic properties of the compounds in Table 1. In the first step, the conformational analysis of the compounds was carried out with Spartan'14 v. 1.1.4 software and the semi-empirical method PM6, seeking the lowest energy conformation. In the second step, the most stable compound was analyzed in the Gaussian 09 software using the functional B3LYP and base 6–311+G(d,p) and IEFPCM methanol as solvent. Next, in the third step, a vibrational analysis (frequency) was performed on the same theoretical level. Finally, in the fourth step, TD-DFT calculations were performed to calculate the energetic transitions and the theoretical UV-vis spectra.

2.3. Experimental Protocol

The absorption profiles were generated by spectrophotometry. Quercetin and resveratrol were used to compare the experimental and theoretical absorption profiles equivalence. To obtain the experimental data, a spectrophotometer was used in the range of 240–400 nm, and a methanol solution of 3.048 mg/L was used for quercetin and 3.06 mg/L for resveratrol.

3. Results and Discussion

After the construction of the compound's structures in GaussView 4 [33], they were submitted to conformational analyses in Spartan'14 [34]. The conformational search by the semi-empirical PM6 method was carried out to select, among all possible 3D conformations, the most stable one, which has the lowest energy [40–43].

The most stable conformation was subjected to DFT calculations, seeking to understand its energy transitions and perform a vibrational analysis, different studies also used DFT for conformational and energy calculations [44,45].

For the DFT methods, functional B3LYP and base 6–311+G(d,p) were used, using the implicit solvent methanol (IEFPCM) in Gaussian 09; the functional B3LYP was used

because it is a functional already consolidated in the prediction of UV-vis. Previous studies by the group, by Garcia 2015, also evaluated the effect of different functionals on theoretical UV-vis predictions, and the one that had the highest accuracy for organic molecules with photoprotective qualities was B3LYP [14,15,39,41,46,47].

In addition to maintaining the use of a validated methodology for the simulation of UV-vis spectra for molecules with photoprotective characteristics, diffusion (+) and polarization (d,p) functions were added. This generates more accurate and reliable data in studies of electronic distribution for conjugated systems [48].

The UV-vis predictions on EMC were performed to acquire the knowledge and skills necessary to execute the calculations and to validate the method using Gaussian 09. Accordingly, the results obtained corroborate with other results previously found by our group [14], which enables us to consider the method validated and appropriate for advancing the project. The UV-vis spectrum obtained shows molar absorptivity, the main electronic transitions (mainly singlet states, also known as absorption bands), and oscillator force (Figure 3).

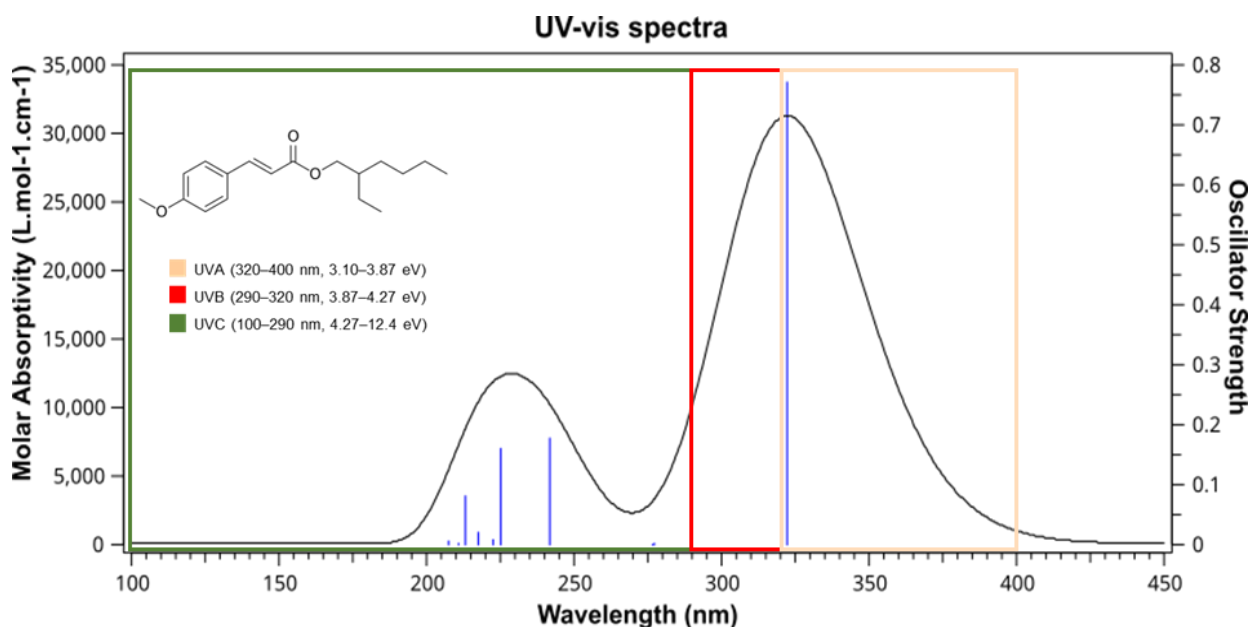


Figure 3. Theoretical UV-vis spectrum of EMC, using the TD-DFT methodology with functional B3LYP, base 6–311+G(d,p), and methanol (IEFPCM) as solvent. Blue lines demonstrate the main electronic transitions (singlets).

Vibrational (frequency) analysis was carried out at the same theoretical level as the geometrical optimizations to confirm the absence of imaginary frequencies. It is essential that the conformation obtained be localized at the minimum energy point with a positive frequency, since negative frequencies show imaginary conformational conditions [24,49]. For the studied compounds, there were no negative frequency implications, showing that the conformational analysis performed using semi-empirical PM6 and DFT methods was adequate and that the conformations were both real and of sufficient quality to advance the study.

The next step was to calculate the electronic properties using the TD-DFT method with functional B3LYP and 6–311+G(d,p) basis sets. These calculations allow us to generate enough data to comprehend the main theoretical electronic states and UV-vis absorption profiles (molecular absorptivity data). Using GaussView 4, the information related to transition energy studies and images of the main electronic transition for each compound and their UV-vis spectra were extracted and are presented in Figure 4 [14].

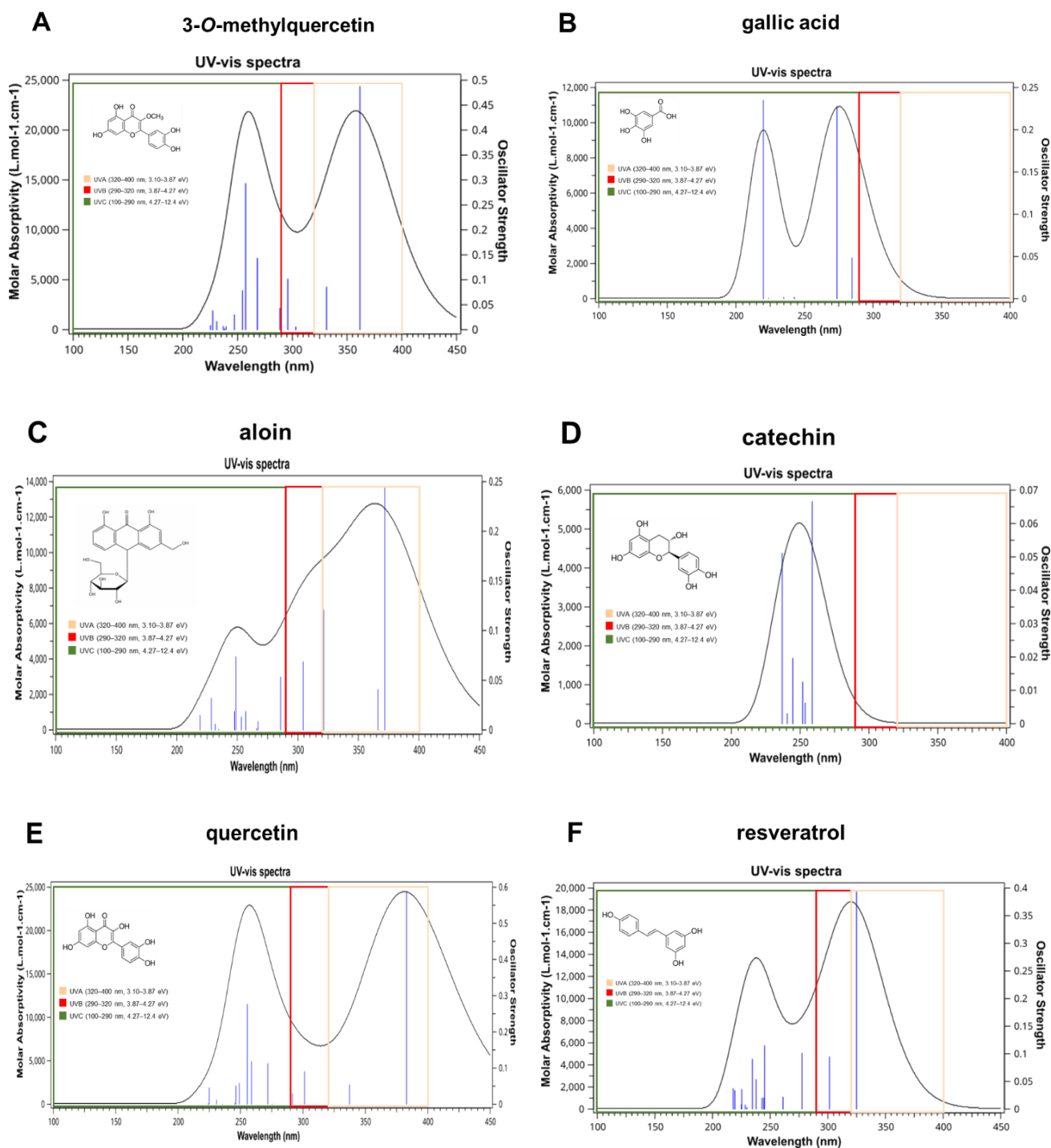


Figure 4. (A–F) Theoretical spectra calculated by TD-DFT for the different compounds. The blue lines show the main electronic transitions (singlets).

The UV-vis prediction results obtained by applying the TD-DFT described method correspond satisfactorily to data obtained through experimental studies found in the literature, with a difference between the theoretical and experimental data ranging between 1 and 5.8% (Table 2).

Table 2. Theoretical λ_{\max} obtained by the work methodology and the experimental λ_{\max} found in the literature and its % error.

Compound	λ_{\max} (nm) Theoretical	λ_{\max} Experimental (Literature)	% Error
3-O-metilquercetina	361.77	358 nm	1
gallic acid	284.74	290 nm	1.8
aloin	371.79	353 nm	5
catechin	258.74	274 nm	5.8
quercetin	383.01	375 nm	2
resveratrol	324.93	307 nm	5.5

The compound 3-O-methylquercetin (Figure 4A) had the lowest error rate in the study. Its theoretical λ_{\max} calculated at 361.77 nm, while experimental studies suggest that its λ_{\max} is 358 nm, presenting an error rate of 1% [50]. Gallic acid (Figure 4B) also had a low error rate; its theoretical λ_{\max} was calculated at 284.74 nm, and experimental studies indicate that its λ_{\max} is 290 nm, showing a difference of 1.8% [51,52]. Aloin (Figure 4C) had its theoretical λ_{\max} at 371.79 nm, and experimental studies suggest that its λ_{\max} is 353 nm, presenting a difference of 5% [53,54]. Catechin (Figure 4D) showed the highest error rate, with a theoretical λ_{\max} of 258.74 nm and an experimental λ_{\max} suggestive of 274 nm; the difference found was 5.8% [55]. Quercetin (Figure 4E) showed great proximity between the results; its theoretical λ_{\max} is 383.01 nm; experimental studies suggest that its λ_{\max} is 375 nm, and the error rate found is 2% [56]. Resveratrol (Figure 4F) has a theoretical λ_{\max} of 324.93 nm, experimental studies in the literature report a λ_{\max} of 307 nm with a 5.5% error rate [57].

A comparison between the previous theoretical studies and the results obtained in this work showed that the methodologies are converging. In these studies, gallic acid was assessed using the functions B3LYP and 6-311+G(d,p) basis sets; in water (IEFPCM) the absorption peak (λ_{\max}) is 275 nm, while our study showed 284 nm (a 3% difference between the results), probably due to the solvent used [47]. For quercetin, the difference between the studies performed by Conard et al. [46] using the B3LYP and 6-31G(d,p) basis sets and methanol (PCM) as solvent was negligible, with about 1% of the calculated absorption peak at 381 nm. Moreover, the theoretical studies performed on resveratrol, again using the B3LYP function with 6-31G* in vacuum, resulted in an absorption peak at 315 nm [58]. In our work, we obtained the λ_{\max} of 324 nm with a difference of 2.8% from previous work, and we attribute this difference to the distinct basis function as well as the solvent employed.

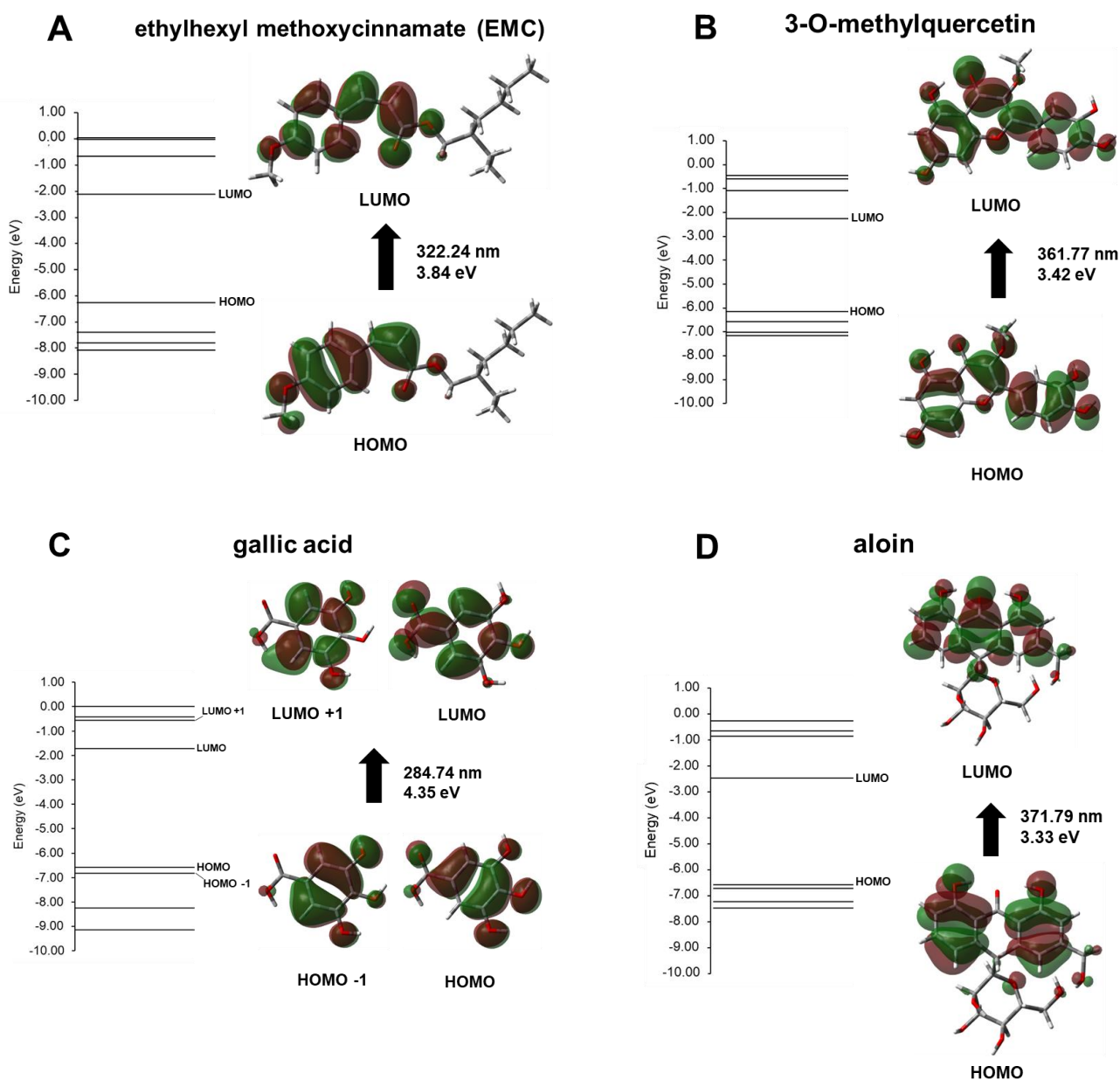
The main electronic transitions calculated by TD-DFT were also analyzed. They demonstrate each orbital's contribution so that the main electronic transition and the area responsible for the molar absorptivity peak (λ_{\max}) can occur.

Using GaussView, it was also possible to calculate the orbital involved in the main electronic transition and obtain the energies from the orbital between HOMO -3 and LUMO +3. The results of the electronic transition, expressed in eV, are presented in Table 3 and were used to generate the graphs in Figure 5. The representations and images were generated in GaussView, demonstrating the orbitals involved in the main electronic transition and the energy necessary for this transition to occur. For all compounds, this transition happens in the near area of the molecule's λ_{\max} , in the UV-vis range.

Generally, most compounds presented a HOMO \rightarrow LUMO transition in λ_{\max} . However, gallic acid presents a contribution in HOMO -1 \rightarrow LUMO and HOMO \rightarrow LUMO +1, and catechin shows a contribution from HOMO -1 \rightarrow LUMO and HOMO -3 \rightarrow LUMO +1.

Table 3. Energy and contribution of molecular orbitals related to electronic transitions calculated using functional B3LYP.

Compound	λ_{\max} (nm)	Energy (eV)	Electronic Transition Contribution (%)
ethylhexyl methoxycinnamate (EMC)	322.24	3.84	H \rightarrow L (+99%)
3-O-methylquercetin	361.77	3.42	H \rightarrow L (+93%) H-1 \rightarrow L (+62%)
gallic acid	284.74	4.35	H \rightarrow L (+27%) H \rightarrow L+1 (+9%)
aloin	371.79	3.33	H \rightarrow L (+98%) H \rightarrow L (+74%)
catechin	258.74	4.79	H-1 \rightarrow L (+9%) H-3 \rightarrow L+1 (+7%)
quercetin	383.01	3.24	H \rightarrow L (+96%)
resveratrol	324.93	3.81	H \rightarrow L (+97%)

**Figure 5.** Cont.

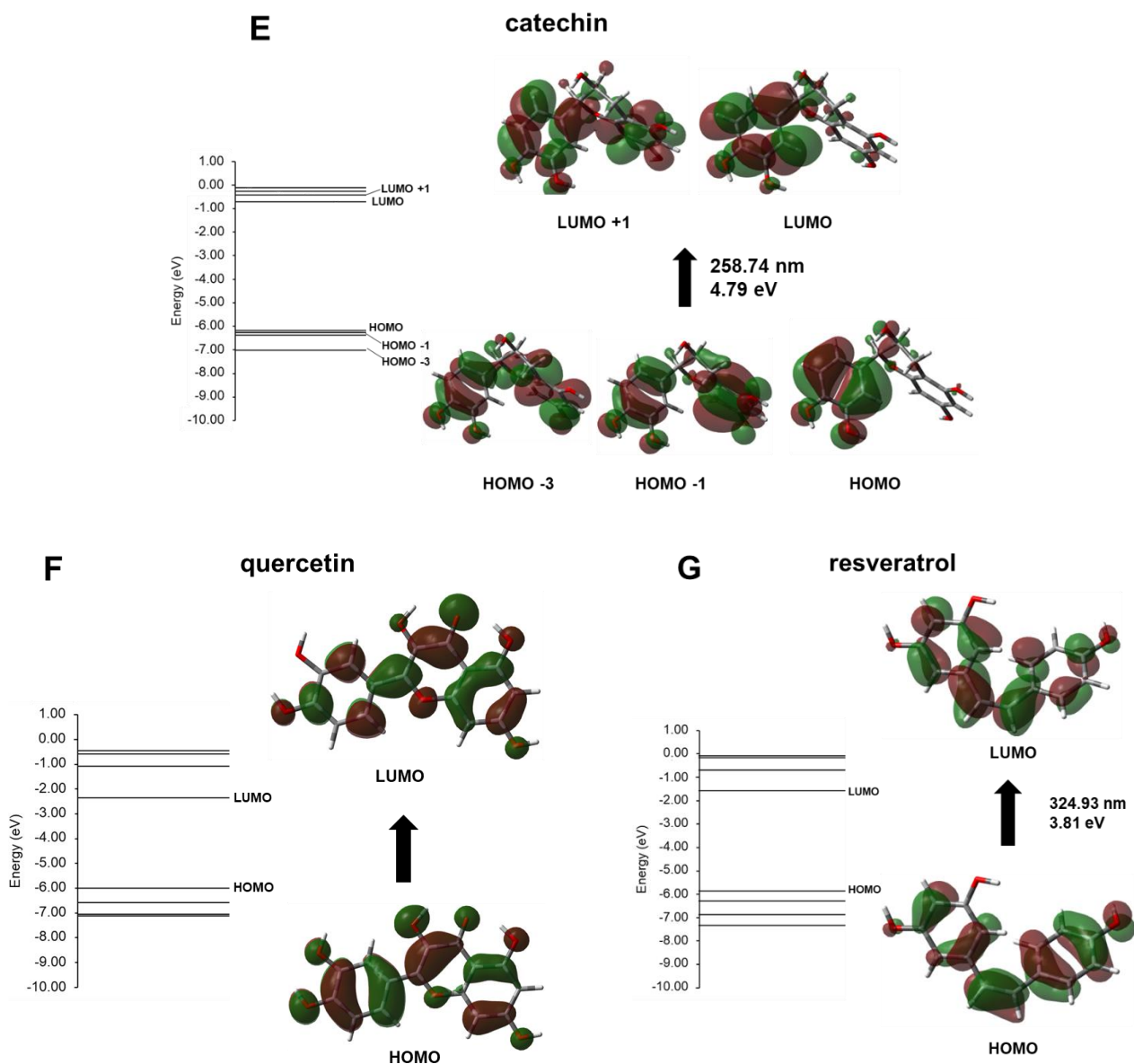


Figure 5. (A–G) Electronic transitions calculated by DFT. These images show the orbitals involved in the transition that are responsible for the molecule's λ_{max} in the UV-vis range and the energy necessary for this transition to occur.

Regarding the compounds studied, this correlation can be observed in the UV-vis graphs generated. The results suggest that the closer the wavelength is to visible light (400 nm), the smaller the energy gap. For catechin (Figure 5E), the calculations show an energy gap of 4.79 eV and λ_{max} of 258.74 nm, which is confirmed by its UV absorption profile, demonstrating that it acts in the UVC range (100–290 nm) (Figure 4D). Quercetin (Figure 4), on the other hand, has shown an energy gap of 3.24 eV and λ_{max} of 383.01 nm, indicating that its highest UV absorption is in the UVA range (320–400 nm) (Figure 4E).

Thus, according to the studies realized in this work, compounds 3-O-methylquercetin (Figure 4A), aloin (Figure 4C), quercetin (Figure 4E), and resveratrol (Figure 4F) show an absorption range similar to EMC (Figure 5B,D,F,G), which implies that they deserve attention and are promising candidates for photoprotection.

The other compounds studied, such as gallic acid (Figure 4B) and catechin (Figure 4D), presented absorption profiles that were mostly in the UVC (100–290 nm) and UVB (290–320 nm) ranges and showed a wider energy gap than the other compounds studied. This indicates that

these molecules might be interesting for chemical sunscreen compositions, along with other compounds that encompass other areas in the UV spectrum.

Thus, these correlated pieces of information can be promising if utilized to better predict the compound's electronic behavior and photoprotective properties.

Experimental Validation

To validate the results, a study of the absorption profiles generated through the experimental protocol for the compounds quercetin and resveratrol was carried out, evaluating whether the absorption profiles would be equivalent to those obtained by the computational protocol (Figure 6).

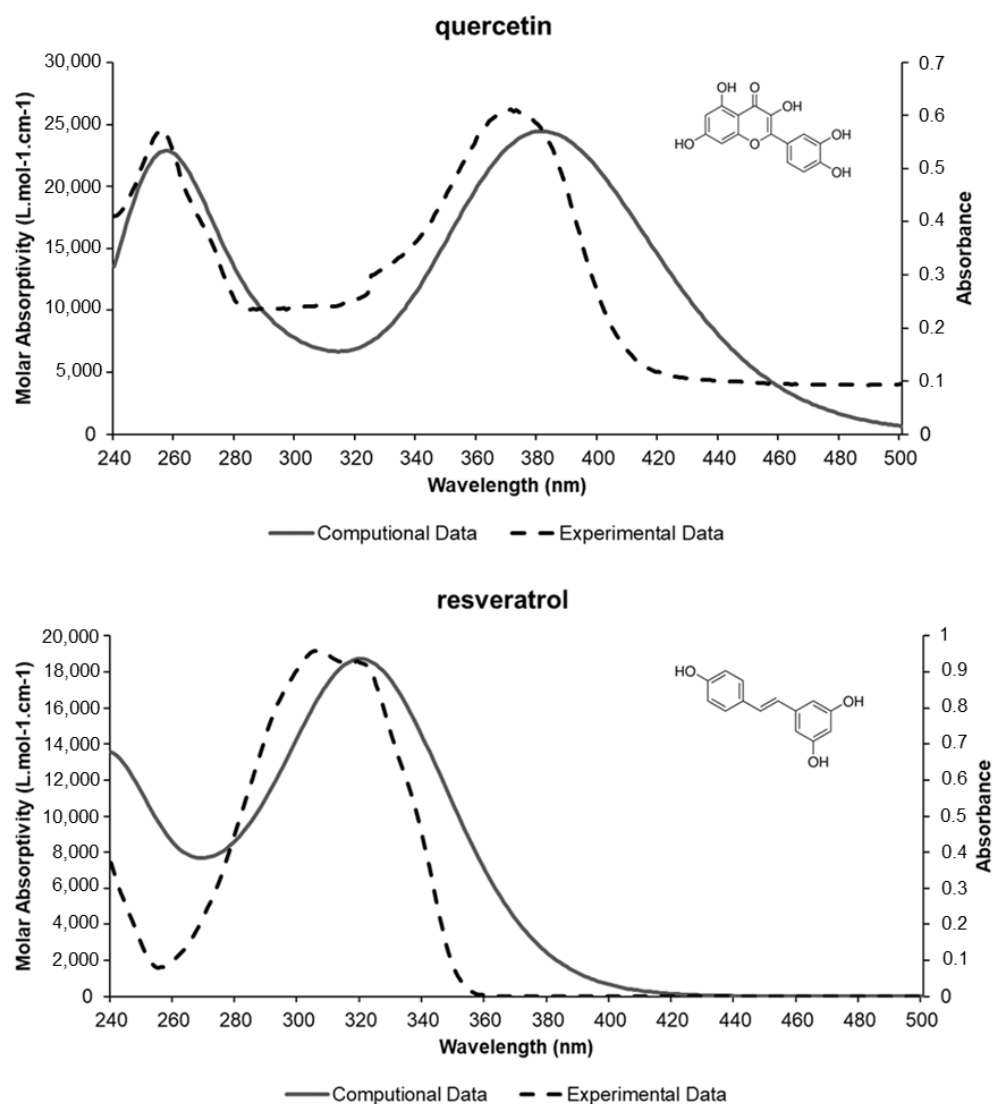


Figure 6. Comparison between quercetin and resveratrol absorption profiles obtained through TD-DFT and the experimental graphs obtained from a scan in a solution of 3.048 mg/L for quercetin and 3.06 mg/L for resveratrol, both using methanol as solvent.

The results obtained from both compounds validate the prediction results of the computational protocol, as both the absorption profiles and the λ_{\max} presented themselves in similar areas of the spectra. For quercetin, the experimental λ_{\max} was located at 371 nm and the theoretical λ_{\max} at 383.01 nm, and for resveratrol, the experimental λ_{\max} was located at 305 nm and the theoretical λ_{\max} at 324.93 nm. These comparative results obtained by experimental and computational techniques are needed to demonstrate that,

even for molecules that differ from each other, the predictive results are within the expected range when analyzing the absorption curves.

4. Conclusions

The aim of this work was to use computational methods, mostly TD-DFT (B3LYP), to simulate different electronic conditions and seek to better understand how the compounds studied act as photoprotective candidates. Examining the UV-vis absorption profiles revealed that the study was quite satisfactory. The HOMO and LUMO electronic transitions for the compounds 3-O-methylquercetin, aloin, gallic acid, catechin, resveratrol, and quercetin showed promising results when evaluating the energy gap and the UV-vis absorption range. The calculated energy gap values correspond to a range of 4 eV, which confirms that the molecules studied have an absorption in the UV region. The experimental protocol for the absorption profiles of quercetin and resveratrol molecules validated the absorption profiles obtained through the computational protocol (TD-DFT).

In conclusion, our study demonstrated, through computational methods, that the UV spectra prediction method is applicable for compounds of natural origin with photoprotective properties, two of which were experimentally validated. Thus, our work opens the possibility of tracking the most promising compounds *in silico*, which can minimize failures in experimental validations and save laboratory resources. However, we highlight the need for additional experimental validations to refine the mathematical calculations and error rates.

Author Contributions: Development of the computational studies, experimental validation, and manuscript—writing, J.O.A.-M.; collaboration in computational studies and manuscript—writing, A.C.G.S.; collaboration in the experimental validation, C.A.S.d.O.P.; support in the mathematical analyses, A.I.Á.B.; analyses and text composition, A.R.B.; project mentor and advisor in the computational studies, results analyses, and text composition, G.H.G.T. All authors have read and agreed to the published version of the manuscript.

Funding: The present work was carried out with the support of the Coordination of Improvement of Higher Education Personnel—Brazil (CAPES), the National Council for Scientific and Technological Development (CNPq 436791/2018-8 and 310232/2017-1), and the São Paulo Research Foundation (FAPESP 2017/25543-8).

Data Availability Statement: Not applicable.

Acknowledgments: Programa de Pós-graduação em Fármaco e Medicamentos; Coordination of Improvement of Higher Education Personnel—Brazil (CAPES); and the National Council for Scientific and Technological Development and São Paulo Research Foundation (FAPESP).

Conflicts of Interest: The authors declare no conflict of interest, financial or otherwise.

References

1. Carr, S.; Smith, C.; Wernberg, J. Epidemiology and Risk Factors of Melanoma. *Surg. Clin. N. Am.* **2020**, *100*, 1–12. [[CrossRef](#)]
2. Simões, M.C.F.; Sousa, J.J.S.; Pais, A.A.C.C. Skin cancer and new treatment perspectives: A review. *Cancer Lett.* **2015**, *357*, 8–42. [[CrossRef](#)] [[PubMed](#)]
3. Leiter, U.; Keim, U.; Garbe, C. Epidemiology of Skin Cancer: Update 2019. *Adv. Exp. Med. Biol.* **2020**, *1268*, 123–139. [[PubMed](#)]
4. Watson, M.; Holman, D.M.; Maguire-Eisen, M. Ultraviolet Radiation Exposure and Its Impact on Skin Cancer Risk. *Semin. Oncol. Nurs.* **2016**, *32*, 241–254. [[CrossRef](#)] [[PubMed](#)]
5. de Araujo, T.S.; de Souza, S.O. Protetores Solares e os efeitos da radiação ultravioleta. *Sci. Plena* **2008**, *4*, 1–7.
6. Guerra, K.C.; Zafar, N.; Crane, J.S. Skin Cancer Prevention. *StatPearls* **2021**, *204*, 87–93.
7. Beani, J.-C. Ultraviolet A-induced DNA damage: Role in skin cancer. *Bull. Acad. Natl. Med.* **2014**, *198*, 273–295.
8. Velasco, M.V.R.; Sarruf, F.D.; Salgado-Santos, I.M.N.; Haroutiounian-Filho, C.A.; Kaneko, T.M.; Baby, A.R. Broad-spectrum bioactive sunscreens. *Int. J. Pharm.* **2008**, *363*, 50–57. [[CrossRef](#)]
9. Dutra, E.A.; Gonçalves da Costa e Oliveira, D.A.; Kedor-Hackmann, E.R.M.; Miritello Santoro, M.I.R. Determination of sun protection factor (SPF) of sunscreens by ultraviolet spectrophotometry. *Rev. Bras. Ciências Farm.* **2004**, *40*, 381–385. [[CrossRef](#)]
10. Gies, P.; Van Deventer, E.; Green, A.C.; Sinclair, C.; Tinker, R. Review of the Global Solar UV Index 2015 Workshop Report. *Health Phys.* **2018**, *114*, 84. [[CrossRef](#)]
11. Flor, J.; Davolos, M.R.; Correa, M.A. Protetores solares. *Quim. Nova* **2007**, *30*, 153–158. [[CrossRef](#)]

12. Schneider, S.L.; Lim, H.W. A review of inorganic UV filters zinc oxide and titanium dioxide. *Photodermatol. Photoimmunol. Photomed.* **2019**, *35*, 442–446. [[CrossRef](#)]
13. Suozzi, K.; Turban, J.; Girardi, M. Focus: Skin: Cutaneous Photoprotection: A Review of the Current Status and Evolving Strategies. *Yale J. Biol. Med.* **2020**, *93*, 55.
14. Garcia, R.D.; Maltarollo, V.G.; Honório, K.M.; Trossini, G.H.G. Benchmark studies of UV-vis spectra simulation for cinnamates with UV filter profile. *J. Mol. Model* **2015**, *21*, 150. [[CrossRef](#)]
15. Corrêa, B.A.M.; Gonçalves, A.S.; de Souza, A.M.T.; Freitas, C.A.; Cabral, L.M.; Albuquerque, M.G.; Castro, H.C.; dos Santos, E.P.; Rodrigues, C.R. Molecular modeling studies of the structural, electronic, and UV absorption properties of benzophenone derivatives. *J. Phys. Chem.* **2012**, *116*, 10927–10933. [[CrossRef](#)]
16. de Oliveira, A.M. *Introdução à Modelagem Molecular para Química, Engenharia e Biomédicas*; Editora Appris: Curitiba, Brazil, 2018; Volume 2, pp. 12–54.
17. Santos, C.B.; Lobato, C.C.; de Sousa, M.A.; Macêdo, W.J.; Carvalho, J.C. Molecular modeling: Origin, fundamental concepts and applications using structure-activity relationship and quantitative structure-activity relationship. *Rev. Theor. Sci.* **2014**, *2*, 91–115. [[CrossRef](#)]
18. Pankin, D.; Smirnov, M.; Povolotckaia, A.; Povolotskiy, A.; Borisov, E.; Moskovskiy, M.; Gulyaev, A.; Gerasimenko, S.; Aksenov, A.; Litvinov, M.; et al. DFT Modelling of Molecular Structure, Vibrational and UV-Vis Absorption Spectra of T-2 Toxin and 3-Deacetylcalonecitrin. *Materials* **2022**, *15*, 649. [[CrossRef](#)]
19. Govindarajan, M.; Karabacak, M.; Suvitha, A.; Periandy, S. FT-IR, FT-Raman, ab initio, HF and DFT studies, NBO, HOMO–LUMO and electronic structure calculations on 4-chloro-3-nitrotoluene. *Spectrochim. Acta Part A Mol. Biomol. Spectrosc.* **2012**, *89*, 137–148. [[CrossRef](#)]
20. Sant’Anna, C.M.R. Molecular modeling methods in the study and design of bioactive compounds: An introduction. *Rev. Virtual Química* **2009**, *1*, 5–20. [[CrossRef](#)]
21. Ye, N.; Yang, Z.; Liu, Y. Applications of density functional theory in COVID-19 drug modeling. *Drug Discov. Today* **2021**, *4*, 93–97. [[CrossRef](#)]
22. Adamo, C.; Jacquemin, D. The calculations of excited-state properties with time-dependent density functional theory. *Chem. Soc. Rev.* **2013**, *42*, 845–856. [[CrossRef](#)]
23. Townsend, P.A.; Grayson, M.N. Density Functional Theory in the Prediction of Mutagenicity: A Perspective. *Chem. Res. Toxicol.* **2020**, *34*, 179–188. [[CrossRef](#)] [[PubMed](#)]
24. Ji, F.; Guo, Y.; Wang, M.; Wang, C.; Wu, Z.; Wang, S.; Wang, H.; Feng, X.; Zhao, G. New insights into ESIPT mechanism of three sunscreen compounds in solution: A combined experimental and theoretical study. *Colloids Surf. B Biointerfaces* **2021**, *207*, 2039. [[CrossRef](#)] [[PubMed](#)]
25. Morocho-Jácome, A.L.; Freire, T.B.; Oliveira, A.C.; Almeida, T.S.; Rosado, C.; Velasco, M.V.R.; Baby, A.R. In vivo SPF from multifunctional sunscreen systems developed with natural compounds—A review. *J. Cosmet. Dermatol.* **2021**, *20*, 729–737. [[CrossRef](#)] [[PubMed](#)]
26. Aburjai, T.; Tayseer, I. Green sunscreens. In *Sunscreens: Source, Formulations, Efficacy and Recommendations*; Rastogi, R.P., Ed.; Nova: Amman, Jordan, 2019; pp. 245–276.
27. Yilmaz, Y.; Toledo, R.T. Major Flavonoids in Grape Seeds and Skins: Antioxidant Capacity of Catechin, Epicatechin, and Gallic Acid. *J. Agric. Food Chem.* **2004**, *52*, 255–260. [[CrossRef](#)] [[PubMed](#)]
28. Nichols, J.A.; Katiyar, S.K. Skin photoprotection by natural polyphenols: Anti-inflammatory, antioxidant and DNA repair mechanisms. *Arch. Dermatol. Res.* **2010**, *302*, 71–83. [[CrossRef](#)]
29. Mishra, A.; Chattopadhyay, P. Herbal cosmeceuticals for photoprotection from ultraviolet B radiation: A review. *Trop. J. Pharm. Res.* **2011**, *10*, 351–360. [[CrossRef](#)]
30. Catelan, T.B.S.; Gaiola, L.; Duarte, B.F.; Cardoso, C.A.L. Evaluation of the in vitro photoprotective potential of ethanolic extracts of four species of the genus *Campomanesia*. *J. Photochem. Photobiol. B Biol.* **2019**, *197*, 111–500. [[CrossRef](#)] [[PubMed](#)]
31. Phadungsaksawasdi, P.; Sirithanabadeekul, P. Ultraviolet filters in sunscreen products labeled for use in children and for sensitive skin. *Pediatr. Dermatol.* **2020**, *37*, 632–636. [[CrossRef](#)]
32. Tsui, M.M.; Chen, L.; He, T.; Wang, Q.; Hu, C.; Lam, J.C.; Lam, P.K. Organic ultraviolet (UV) filters in the South China sea coastal region: Environmental occurrence, toxicological effects and risk assessment. *Ecotoxicol. Environ. Saf.* **2019**, *181*, 26–33. [[CrossRef](#)]
33. Frisch, M.; Trucks, G.; Schlegel, H.E.; Scuseria, G.W.; Robb, M.A.; Cheeseman, J.R.; Montgomery, J.A., Jr.; Vreven, T.K.; Kudin, K.N.; Burant, J.C.; et al. *Gaussian 03, Revision C. 02*; Gaussian, Inc.: Wallingford, CT, USA, 2004.
34. *Spartan’14*; Wavefunction, Inc.: Irvine, CA, USA, 2013.
35. Becke, A.D. Density-functional exchange-energy approximation with correct asymptotic behavior. *Phys. Rev. A Gen. Phys.* **1988**, *38*, 3098–3100. [[CrossRef](#)] [[PubMed](#)]
36. Miehlich, B.; Savin, A.; Stoll, H.; Preuss, H. Results obtained with the correlation energy density functionals of Becke and Lee, Yang and Parr. *Chem. Phys. Lett.* **1989**, *157*, 200–206.
37. Lee, C.; Yang, W.; Parr, R.G. Development of the Colle-Salvetti correlation-energy formula into a functional of the electron density. *Phys. Rev. B Condens. Matter.* **1988**, *37*, 785–789. [[CrossRef](#)]
38. Frisch, M.J.; Trucks, G.W.; Schlegel, H.B.; Scuseria, G.E.; Robb, M.A.; Cheeseman, J.R.; Scalmani, G.; Barone, V.; Mennucci, B.; Petersson, G.; et al. *Gaussian 09, Revision D. 01*; Gaussian, Inc.: Wallingford, CT, USA, 2009.

39. Trossini, G.H.G.; Maltarollo, V.G.; Garcia, R.D.; Pinto, C.A.S.O.; Velasco, M.V.R.; Honorio, K.; Baby, A. Theoretical study of tautomers and photoisomers of avobenzene by DFT methods. *J. Mol. Model.* **2015**, *8*, 104–107. [CrossRef]
40. Carvalho, I.; Pupo, M.T.; Borges, Á.D.L.; Bernardes, L.S.C. Introdução a modelagem molecular de fármacos no curso experimental de química farmacêutica. *Quim. Nova.* **2003**, *26*, 428–438. [CrossRef]
41. Basavaraj, S.; Hanagodimath, S.M.H. UV-Visible Spectra, HOMO-LUMO Studies on Coumarin Derivative Using Gaussian Software. *AIP Conf. Proc.* **2020**. Available online: https://www.researchgate.net/profile/Shivaleela-Basavaraj/publication/344597213_UV-Visible_Spectra_HOMO-LUMO_Studies_on_Coumarin_Derivative_Using_Gaussian_Software/links/5f833eed458515b7cf79d62f/UV-Visible-Spectra-HOMO-LUMO-Studies-on-Coumarin-Derivative-Using-Gaussian-Software.pdf (accessed on 2 July 2021).
42. Minenkov, Y.; Sharapa, D.I.; Cavallo, L. Application of Semiempirical Methods to Transition Metal Complexes: Fast Results but Hard-to-Predict Accuracy. *J. Chem.* **2018**, *14*, 3428–3439. [CrossRef]
43. Sikorska, C.; Puzyn, T. The performance of selected semi-empirical and DFT methods in studying C60 fullerene derivatives. *Nanotechnology* **2015**, *26*, 455702. [CrossRef]
44. Christina Jebapriya, J.; Christian Prasana, J.; Muthu, S.; Fathima Rizwana, B. Spectroscopic (FT-IR and FT-Raman), quantum computational (DFT) and molecular docking studies on 2(E)-(4-N,N-dimethylaminobenzylidene)-5-methylcyclohexanone. *Mater. Today Proc.* **2022**, *50*, 2695–2702. [CrossRef]
45. Rad, A.S.; Ardjmand, M.; Esfahani, M.R.; Khodashenas, B. DFT calculations towards the geometry optimization, electronic structure, infrared spectroscopy and UV-vis analyses of Favipiravir adsorption on the first-row transition metals doped fullerenes; a new strategy for COVID-19 therapy. *Spectrochim. Acta Part A Mol. Biomol. Spectrosc.* **2021**, *247*, 119082. [CrossRef]
46. Cornard, J.P.; Dangleterre, L.; Lapouge, C. Computational and Spectroscopic Characterization of the Molecular and Electronic Structure of the Pb(II)–Quercetin Complex. *J. Phys. Chem.* **2005**, *109*, 10044–10051. [CrossRef]
47. Martin, C.; Bruneel, J.-L.; Castet, F.; Fritsch, A.; Teissedre, P.-L.; Jourdes, M.; Guillaume, F. Spectroscopic and theoretical investigations of phenolic acids in white wines. *Food Chem.* **2017**, *221*, 568–575. [CrossRef]
48. Millot, M.; Di Meo, F.; Tomasi, S.; Boustie, J.; Trouillas, P. Photoprotective capacities of lichen metabolites: A joint theoretical and experimental study. *J. Photochem. Photobiol. B Biol.* **2012**, *111*, 17–26. [CrossRef]
49. Ochterski, J.W. Vibrational Analysis in Gaussian. 2020. Available online: <https://gaussian.com/vib/> (accessed on 2 July 2021).
50. Antunes-Ricardo, M.; Gutiérrez-Urbe, J.A.; Guajardo-Flores, D. Extraction of isorhamnetin conjugates from *Opuntia ficus-indica* (L.) Mill using supercritical fluids. *J. Supercrit. Fluids* **2017**, *119*, 58–63. [CrossRef]
51. Dharmender, R.; Madhavi, T.; Reena, A.; Sheetal, A. Simultaneous Quantification of Bergenin, (+)-Catechin, Gallicin and Gallic acid; and Quantification of β -Sitosterol using HPTLC from *Bergenia ciliata* (Haw.) Sternb. *Forma ligulata* Yeo (Pasanbheda). *Pharm. Anal. Acta* **2010**, *1*, 1000104. [CrossRef]
52. Song, H.; Chen, C.; Zhao, S.; Ge, F.; Liu, D.; Shi, D.; Zhang, T. Interaction of gallic acid with trypsin analyzed by spectroscopy. *J. Food Drug Anal.* **2015**, *23*, 234–242. [CrossRef]
53. Burmistrova, N.A.; Krivets, O.O.; Monakhova, Y.B. UV Spectroscopic Determination of Aloin in Aloe vera (*A. vera*) Samples Based on Chemometric Data Processing. *J. Anal. Chem.* **2020**, *75*, 1137–1142. [CrossRef]
54. Logaranjan, K.; Devasena, T.; Pandian, K. Quantitative Detection of Aloin and Related Compounds Present in Herbal Products and Aloe vera Plant Extract Using HPLC Method. *Am. J. Anal. Chem.* **2013**, *4*, 600–605. [CrossRef]
55. Ibrahim, Y.M.; Musa, A.; Yakasai, I.A. Spectrophotometric method for determination of catechins in green tea and herbal formulations. *Niger. J. Pharm. Sci.* **2017**, *16*, 25–30.
56. Golonka, I.; Wilk, S.; Musiał, W. The Influence of UV Radiation on the Degradation of Pharmaceutical Formulations Containing Quercetin. *Molecules* **2020**, *25*, 5454. [CrossRef]
57. Réka-Anita, D.; Chis, V. Conformational Space and Electronic Absorption Properties of the Two Isomers of Resveratrol. *Stud. Univ. Babeş-Bolyai Phys.* **2018**, *62*, 52–57.
58. Sheikhi, M.; Shahab, S.; Khaleghian, M.; Hajikolaee, F.H.; Balakhanava, I.; Alnajjar, R. Adsorption properties of the molecule resveratrol on CNT(8,0-10) nanotube: Geometry optimization, molecular structure, spectroscopic (NMR, UV/Vis, excited state), FMO, MEP and HOMO-LUMO investigations. *J. Mol. Struct.* **2018**, *1160*, 479–487. [CrossRef]

Disclaimer/Publisher’s Note: The statements, opinions and data contained in all publications are solely those of the individual author(s) and contributor(s) and not of MDPI and/or the editor(s). MDPI and/or the editor(s) disclaim responsibility for any injury to people or property resulting from any ideas, methods, instructions or products referred to in the content.